

Check for updates



Preparation and Analysis of High-Performance Thermoplastic Composites

Péter Széplaki¹ | Szabolcs Hajagos¹ | Szabolcs Krizsma¹,² | Béla Zink¹,² | András Suplicz¹,² 🕞

¹Department of Polymer Engineering, Faculty of Mechanical Engineering, Budapest University of Technology and Economics, Budapest, Hungary | ²MTA-BME Lendület Lightweight Polymer Composites Research Group, Budapest, Hungary

Correspondence: András Suplicz (suplicz@pt.bme.hu)

Received: 22 April 2025 | Revised: 30 June 2025 | Accepted: 22 July 2025

Funding: This work was supported by the National Research, Development and Innovation Office, Hungary (OTKA FK 138501). Project no. RRF-2.3.1-21-2022-00009, titled National Laboratory for Renewable Energy, has been implemented with the support provided by the Recovery and Resilience Facility of the European Union within the framework of Programme Széchenyi Plan Plus. This research was funded by the Horizon Europe Framework Programme and the call HORIZON-WIDERA-2021-ACCESS-03 under the grant agreement for project 101079051-IPPT_TWINN. Project no. KDP-IKT-2023-900-II-00000957/0000003 has been implemented with the support provided by the Ministry of Culture and Innovation of Hungary from the National Research, Development and Innovation Fund, financed under the KDP-2023 funding scheme. Project no. TKP-6-6/PALY-2021 has been implemented with the support provided by the Ministry of Culture and Innovation Fund, financed under the TKP2021-NVA funding scheme. This paper was supported by the János Bolyai Research Scholarship of the Hungarian Academy of Sciences (MTA).

Keywords: carbon fiber | mechanical properties | polyamide 6 | thermal properties | thermoplastic composite | T-RTM technology

ABSTRACT

As the plastics industry continues to grow, the amount of plastic waste increases. The European Union is trying to reduce the amount of plastic waste through various actions. Recycling is perhaps the best way to achieve this. The importance of polymer composites has increased dramatically, and thanks to the spread of thermoplastic resin transfer molding (T-RTM), composites can be produced very efficiently. This is because \$\epsilon\$-caprolactam, the monomer of polyamide 6 (PA6), can be processed at low pressures like epoxy or any other thermoset resin due to its low viscosity. PA6 is produced from \$\epsilon\$-caprolactam, activator, and catalyst by in situ ring-opening polymerization in a temperature-controlled mold with sufficiently short cycle times. We produced carbon fiber-reinforced composite sheets with PA6 as the matrix material by T-RTM. A special vertical injection molding machine and the corresponding in situ unit were used for the experiments. We investigated the mechanical, thermal, and morphological properties of continuous carbon fiber-reinforced composites—we performed mechanical and thermal tests on the samples and compared the results with the properties of reference sheets produced from the matrix material. Our goal was to produce high-quality and properly impregnated composite products suitable for engineering applications. Exploring these relationships is essential for creating components with high aesthetic value, which can be used in visible locations in addition to their load-bearing role.

1 | Introduction

Global plastics production was around 413.3 million tons in 2023, 8% of which was used by the automotive industry. Polyamides are widely used engineering polymers today. In the European Union, the demand for polyamides (PA) in 2022 was

approximately 1 million tons due to their excellent engineering and mechanical properties [1].

The keys to mass production are a fast production cycle and consistently high product quality. In the 21st century, recyclability and energy use have also become factors of paramount

This is an open access article under the terms of the Creative Commons Attribution-NonCommercial-NoDerivs License, which permits use and distribution in any medium, provided the original work is properly cited, the use is non-commercial and no modifications or adaptations are made.

© 2025 The Author(s). Polymer Composites published by Wiley Periodicals LLC on behalf of Society of Plastics Engineers.

Summary

- PA6/CF composites were produced via anionic ringopening polymerization.
- We achieved high-quality impregnation of reinforcements.
- Tensile strength was seven times higher than the
- HDT was over 300% higher than that of the reference sample.
- We developed a short-cycle, scalable process for industrial use.

importance, which justify the use of thermoplastic composites. The greatest drawback of these materials is the high viscosity of the matrix $(10-100 \, \text{Pa} \cdot \text{s})$ because the impregnation of continuous fibers is problematic [2, 3].

Using ε-caprolactam and in situ polymerization addresses this problem. In the anionic ring-opening polymerization (AROP) of caprolactam (CL), initiation begins with the deprotonation of CL monomers by the initiator, forming negatively charged, activated monomers. These anionic monomers attack neutral monomers, opening their rings and forming new reactive species. A rapid charge rearrangement follows, generating nitrogen-acyllactam growth centers. This initiation phase is followed by propagation, where activated monomers successively react with the growing chain ends, elongating the polymer. The concentration of the activated monomer remains nearly constant, and propagation continues until thermodynamic equilibrium is reached between monomer and polymer [4]. Initiator and activator systems are also added to the formula to promote polymerization [5-7]. For this process, anionic initiators are typically used, most commonly sodium caprolactam (C10) or magnesium bromide caprolactam (C1). The activator can be direct or indirect, with isocyanates commonly used as indirect activators. Activator solutions are prepared like initiator solutions, but hexamethylene-1,6-carbamoyl caprolactam (C20P) or N-acetylcaprolactam (Activator0) are used in the literature, mixed with dry caprolactam. The most common initiator-activator pair is C10-C20P [8].

The continuous reinforcing material can be impregnated properly due to the low melt viscosity of the ϵ -caprolactam (3–5 mPa·s) [9–11]. Also, because of the low melt viscosity, this technology offers short cycle time at low pressures. It allows the production of load-bearing composite parts with different layer orders, which helps customize the loads. Furthermore, one of the most important features of this technology is that the products have a thermoplastic matrix; therefore, they are recyclable [12–15].

Since in situ AROP is used to produce the matrix material, optimizing this process also significantly improves the quality of the product. Choi et al. [16] investigated how polymerization conditions impact mechanical properties. They concluded that the mixing ratio of the activator and the catalyst is the main factor influencing tensile strength. Their results indicated that the

amount of the C10 activator should be above 1.89 wt%, and the amount of the C20 catalyst should be between 1.89 and 3.5 wt% for the best mechanical properties. Kim et al. [17] also optimized the catalyst and activator content, but they also investigated the ideal processing temperature and its effect in the range of 130°C to 150°C. They found that the ideal temperature was between 140°C and 150°C. At lower temperatures, the reaction did not proceed properly despite the high activator ratio, and at higher temperatures it proceeded too fast, leading to impaired mechanical properties. In addition, when nanomaterials (NMs) and plasma treatment were used simultaneously in the T-RTM process, cycle time was reduced, and mechanical properties significantly improved. The effect of processing temperature was investigated by Li et al. [18]. They prepared carbon fiber-reinforced composites with a polyamide 6 matrix by in situ polymerization with vacuum-assisted casting (VARTM). They found that the optimal temperature range for polymerization was between 140°C and 160°C. The reason was that the conversion rate was the highest in this temperature range, giving the best mechanical properties.

Moisture content is critically important in T-RTM production, as moisture significantly influences product quality. Several methods have recently been developed to overcome the problem of moisture. Wilhelm et al. [19] found that the negative effect of moisture in the air can be easily eliminated by increasing the concentration of activator and catalyst in the formula. Lee et al. [20] tried a different approach; they improved the properties of the mixture by adding zeolite. By exploiting the selective water absorption effect of zeolite, they reduced drying time and the quality variation caused by the change in moisture content in the composite. They performed mechanical tests on the carbon fiber–reinforced composites they produced with and without zeolite and concluded that zeolite does not impair mechanical properties.

Dencheva et al. [21] investigated the production of PA6-based thermoplastic laminate composites reinforced with glass fiber or PA66 fabric via in-mold AROP of ε-caprolactam. The method produced high monomer conversion and enhanced the mechanical properties of the composites. Structural analyses confirmed good fiber-matrix adhesion and crystallinity variations. The study demonstrates the feasibility and industrial potential of producing high-performance PA6 composites through efficient in situ polymerization. Dencheva et al. [22] investigated the structure-property relationships in single polymer composites (SPCs) based on polyamide-6 (PA6), prepared via the in-mold AROP of ε-caprolactam in the presence of PA6 textile fibers. They examined how fiber content, surface treatment, and polymerization temperature affect the crystalline structure and mechanical properties. The formation and morphology of a transcrystalline layer (TCL) at the fiber/matrix interface were analyzed by SEM, PLM, and synchrotron WAXS. The study demonstrates that desizing the fibers leads to stronger fiber-matrix adhesion, thinner TCLs, and improved mechanical performance. These findings highlight the potential of AROP for producing recyclable, high-performance thermoplastic composites.

It is interesting to compare the properties of thermoplastic composite materials with those of composites with classical epoxy

and other thermosetting matrix materials. Murray et al. [23] compared the impact behavior of carbon fiber (CF)/anionic polyamide 6 (APA-6) and CF/epoxy using the same fabric, layer order, and tool cavity. The results showed that CF/APA-6 absorbed ~21% more energy before fracture, induced ~7% less force, and the damaged area was one-third less. In all aspects, the APA-6 matrix outperformed the epoxy matrix. In another study, Murray et al. [24] produced high-quality glass fiber PA-6 composite laminates. Mechanical and chemical studies showed that the material properties of the laminates were highly comparable to commercially available glass fiber products, and the cost of the production equipment is low. They demonstrated the massive potential of using APA-6 as a matrix, and their results can significantly contribute to the broader use of APA-6 composites in various industries.

In addition to the low viscosity of the matrix material, it is of paramount importance that the permeability of the reinforcing fabric is also adequate for good impregnability. Such research for T-RTM technology has not been carried out yet; although Gomez et al. [25] investigated the effect of the permeability of the reinforcing fabric on mechanical properties. They found the optimal parameters by gradually increasing the applied pressure from 3.6 bar to 15 bar during the impregnation phase to ensure complete impregnation without causing significant fiber movement. Flexural strength increased at higher impregnation pressures, with a 51.8% increase at 10 bar.

In the past, several studies have been written on the fabrication and testing of continuous carbon fiber-reinforced composite structures with a PA6 matrix. However, the authors have mostly investigated only one property of the specimens; comprehensive mechanical, thermal, and dynamic tests were not performed. We provide a comprehensive picture of the properties of these composites through a complex, full-scale study. We produced PA6-CF composite samples on industrial equipment with controlled parameters, as opposed to previous production methods in the literature typically based on vacuum infusion molding or prototype equipment. This method produces a product of the same quality as large-scale production. Its properties can be analyzed and more accurately tested, and the results are also more reproducible. Proper impregnation of the carbon fabric is essential for good properties of the composite. Therefore, we carried out a detailed analysis of permeability, where we investigated the relationship between the permeability and impregnability of the reinforcement for different layer numbers. In addition, the prepared samples were subjected to comprehensive tests, including quasi-static, dynamic, and thermal tests, fiber content analysis, and microscopic examination.

2 | Materials and Methods

2.1 | Materials

The matrix was prepared from a system of ϵ -caprolactam, C10 (sodium caprolactamate) and C20P (hexamethylene-1,6-dicarbamoyl caprolactam). The mixing ratio was 90:6:4 m% (93.6:5.2:1.2 mol%). The ratio was based on our previous studies and the manufacturer's recommendation. This was optimized for producing the PA6 with AROP with a short cycle time below

its melting point (between 130°C and 170°C). The melting point of the AP-Nylon ϵ -caprolactam (CL, L. Brüggemann GmbH & Co. KG, Heilbronn, Germany) was 69°C , with a density of 1.02g/cm^3 in the molten state and a viscosity very similar to that of water (3–5 mPa·s). The initiator in the formula was sodium caprolactamate (Brüggolen C10, L. Brüggemann GmbH & Co KG, Heilbronn, Germany) with a melting point of 62.2°C and a density of 1.02g/cm^3 in the molten state. The activator was hexamethylene-1,6-dicarbamoyl caprolactam (Brüggolen C20P, L. Brüggemann GmbH & Co. KG, Heilbronn, Germany). Its melting point is 70°C , and its density is 1.02g/cm^3 in the molten state.

The reinforcing structure was from PX35 carbon fibers (filament count: 50k) manufactured by Zoltek Zrt. (Hungary). In the X-C-305 fabric (prepared by SAERTEX GmbH & Co.KG, Germany), these carbon fibers were in a $+45^{\circ}/-45^{\circ}$ non-crimp, biaxial arrangement. The areal density of the fabric was $305\,\mathrm{g/m^2}$. The diameter of the elementary fibers was $7.2\,\mu\mathrm{m}$. The sizing was optimized for PA6-based thermoplastic composites. The fabrics were cut to mold size with electric shears.

2.2 | Preparation of Samples

The flat specimens $(200\,\text{mm}\times375\,\text{mm}\times2\,\text{mm})$ were prepared with a T-RTM machine by in situ AROP. We used a vertical Engel Insert $200\,\text{V}/200\text{H}/80$ injection molding machine and the corresponding D60 in situ unit (ENGEL Austria GmbH, Schwertberg, Austria). The structural design of the machine is shown in Figure 1. Its unique feature is that the activator and initiator components are only mixed in the mold, in a dynamic mixing head.

The first step (1) of the production cycle (Figure 1b) is to cut the appropriate reinforcing fabrics, assemble the reinforcing structure, preform it if necessary, and then insert the preformed reinforcing material into the mold. In the second step (2), the mold is closed to the vacuuming position, and a vacuum is built up in the cavity (~900 mbar). In this position, the cavity is hermetically sealed from the environment. The vacuum helps to remove air and moisture from the cavity, which inhibit polymerization. The vacuum also ensures the best possible filling of the mold. After that, the mold is closed completely to seal the vacuum holes. Next, the infiltration of the reinforcing fabric begins. The injection unit starts the injection cycle of the monomer or oligomer and the corresponding catalyst or activator (3). The individual components are melted in separate containers so that polymerization is not initiated prematurely. When the components are in the melt state, they are transferred to the heated mold (155°C) via heated tubes. The melt is metered and fed into the mold by pistons. The components are mixed by a dynamic mixing head. In the mixing head, the melted material streams from the two tanks meet through the simultaneously open needle valves, and the flow results in dynamic mixing. A mixing head transfers and mixes the material streams; then, the materials are injected into the tempered mold. Once injection is complete, polymerization starts while the clamping force is maintained. The pressure in the mold cavity decreases as the product shrinks due to polymerization and crystallization (4).

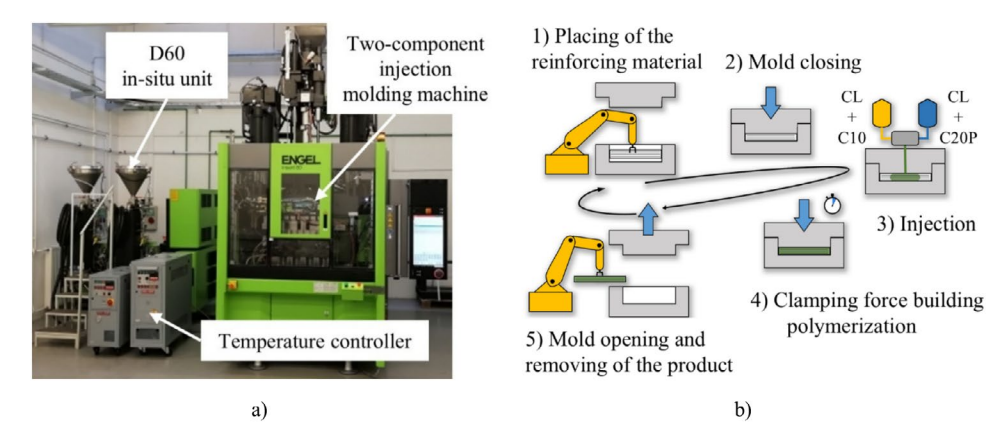


FIGURE 1 | Engel insert 200V/200H/80 injection molding machine and the corresponding in situ unit D60 (a) and the T-RTM technology flow-chart (b).

In contrast to the time-consuming cross-linking process of cross-linked resins, the in situ polymerization and solidification of thermoplastic composites occurs within a few minutes. It takes less than 5 min to reach above 99% conversion; that is, polymerization time is 5 min. This time value was based on our previous research and literature data [26, 27], where the process took less time, but we added a safety margin, so we used 5 min. The machine also melts and doses the material required for the next injection during this time. After polymerization time has elapsed, the mold opens (5), and the product can be removed manually or robotically. The T-RTM technology is highly automatable, making it suitable for mass production with good quality for the automotive industry. High reinforcement content is possible, and no post-processing of the finished product is required [2, 28–31].

The nominal thickness of the mold cavity is 2 mm, which can vary slightly due to the flexible silicone seals in the parting line. The parameters of the production cycle are summarized in Table 1.

First, the reinforcement structure was cut to the shape and size $(205\times375\,\mathrm{mm})$ of the cavity. In the fabrication process, 2 (CF2), 4 (CF4), and 6 (CF6) layers of the biaxial fabric were used. The average thickness of one layer was 0.4 mm. The layout was symmetrical to eliminate warpage as much as possible. Still, samples with two layers often produced significant warpage. The warpage in the CF2 specimen may be caused by its asymmetric structure. On one side of the sample (typically the top), there was a thicker matrix layer due to the geometry of the mold. The matrix and the reinforcement have different thermal expansion and the matrix shrinks during polymerization and crystallization. Thus, due to the greater dimensional change of the matrix, the product warped toward the matrix-rich side.

The quality of the 2-, 4-, and 6-layer samples differed greatly. Figure 2 clearly shows that in the case of the 2-layer samples, there is a thicker matrix layer on top of the reinforcement structure. Also, in the 6-layer samples, the six layers of fabric were too dense because of the high clamping force, and the matrix material did not impregnate the center of the plate. Instead, it flowed around the fabric and entered it from the sides. The poor fill could also have been caused by the matrix material starting to flow around the edge of the mold in the direction of lower resistance, thus flowing around the fabric and trapping air. For this

TABLE 1 | Parameters of the T-RTM cycle.

Parameters	Values	
In situ melting tank temperature	120°C	
Mixing head temperature	155°C	
Mold temperature	155°C	
Sprue temperature	155°C	
Dosage volume	130 cm ³ /component	
Injection volume without fiber	90 cm ³ /component	
Injection volume with fiber	73 cm ³ /component	
Injection pressure limit	80 bar	
Injection speed	7 cm ³ /s/component	
Clamping force	80 t	
Polymerization time	300 s	
Mold vacuum	900 mbar	

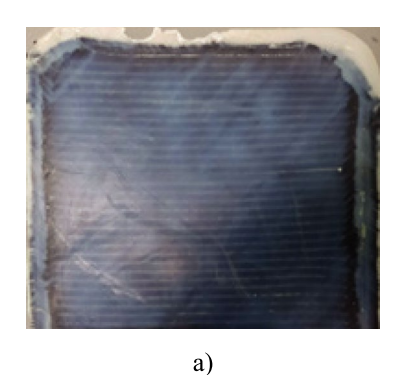
reason, the samples from the 6-layer sheets were cut out from the gating zone. Hence, the mechanical and thermal properties were tested mainly on the 4-layer samples, which had the best quality.

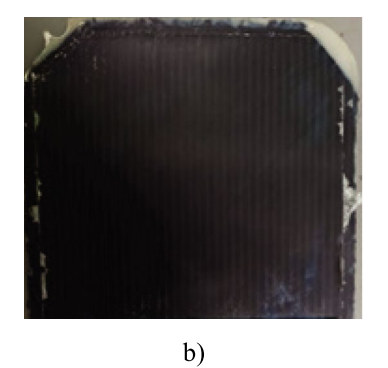
2.3 | Characterization of the Samples

2.3.1 | Fiber Content

The fiber content ($X_{\rm fc}$) of the samples was determined; the pieces were placed in ceramic cups for each type of composite material. The weight of both the empty ($m_{\rm c}$) and filled cups ($m_{\rm s}$) was measured, and the cups were placed in an annealing furnace (Denkal 6B, Kalória Hőtechnikai Ltd.), where the matrix material was burnt out at 550°C for 4h. After that, the mass of the cups was measured with the remaining fiber ($m_{\rm sb}$). Fiber content was calculated with Equation (1), where the results were compensated for with the ash content of the matrix.

$$X_{\text{fc}}[\%] = \left(\frac{(m_{\text{sb}} - m_{\text{c}})}{(m_{\text{s}} - m_{\text{c}})}\right) \cdot 100 - X_{PAmx}$$
 (1)





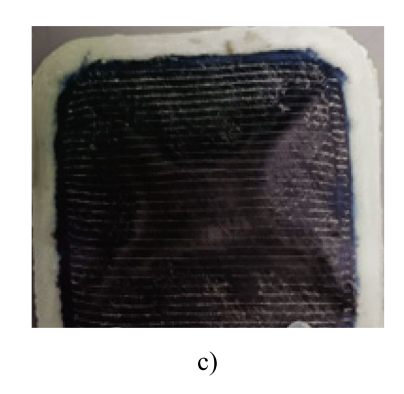


FIGURE 2 | 2- (a), 4- (b), and 6-layer (c) samples.

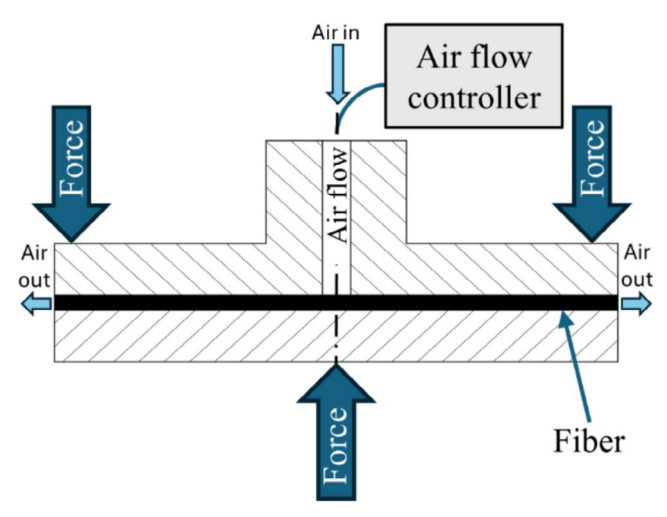


FIGURE 3 | The measurement setup for permeability measurement.

2.3.2 | Permeability Tests

200-mm diameter pure fabric specimens were cut out for the test and inserted between discs in the tensile testing machine (Figure 3). In this in-plane permeability test, air first enters through the upper disc and exits at the edge of the reinforcement through its structure. The instrument displays the relative pressure difference between the internal and ambient air pressure at the set flow rate. From these pressure differences, we calculated the permeability (K) of the material with Equation (2) [32]:

$$K = \frac{\mu Q}{\Delta P 2\pi d} \ln \left(\frac{r}{r_o} \right) \tag{2}$$

where Q is the average flow rate of the medium, ΔP is the pressure difference ($\Delta P = (P_0 - P_r)$), d is the depth of the cavity, r is the radius of the disk, and r_0 is the radius of the inflow hole. μ is the viscosity of air, which can be written with Equation (3) [33].

$$\mu = \mu_{\text{ref}} \left(\frac{T_{\text{ref}} + C}{T + C} \right) \left(\frac{T}{T_{\text{ref}}} \right)^{3/2} \tag{3}$$

where μ is the viscosity of the air at temperature T, $\mu_{\rm ref}$, and $T_{\rm ref}$ are reference values (e.g., $\mu_{\rm ref} = 1.81 \times 10^5$ Pas at $T_1 = 293$ K) and C = 117 K is the so-called Sutherland constant.

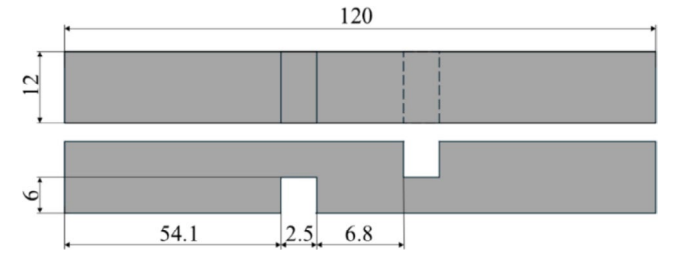


FIGURE 4 | Inter-laminar shear test samples in top and side view.

2.3.3 | Tensile Tests

Five $0/90^{\circ}$ (CF2_90, CF4_90, CF6_90) and five $\pm 45^{\circ}$ test specimens (CF2_45, CF4_45, CF6_45) were cut for each sample type on a Mutronic circular saw cutting table ($2\times25\times250\,\mathrm{mm}$) according to ISO 527-1:2019. During the test, the specimens were gripped at both ends and loaded at a constant speed under measurement conditions specified in the standard (temperature, moisture content). The tensile force as a function of length change was measured and recorded. The test was continued until the specimen ruptured.

A Zwick Z250 tensile testing machine was used with a 250 kN load cell and a 100 kN tensile head. Test speed was 2 mm/min and 5 mm/min for 0/90° and ±45° specimens, respectively. The initial spacing between the tensile heads was 110 mm. The tensile force was recorded until rupture. The elongation of the specimens was determined with a Mercury Monet (Sobriety, Kurim, Czech Republic) optical strain measuring system based on digital image correlation (DIC). The equipment had a 5 MPixel IDS U3-3080CP-P-GL (Imaging Development Systems Inc., Obersulm, Germany) camera and two LED lights.

2.3.4 | Interlaminar Shear Test

In the interlaminar shear test, the $12 \times 120 \,\mathrm{mm}$ specimens were notched on opposite sides in 2 places, 6.8 mm apart, and 3.4 mm from the middle of the sample (Figure 4). Both notches were half the thickness of the specimen. With this design, when the sample was pulled, the layers slid over each other, allowing the properties of the matrix between the layers to be investigated. The interlaminar shear tests were also carried out with the Zwick Z250 universal tensile testing

machine and the associated Sobriety Mercury Monet DIC optical strain gauge.

2.3.5 | Falling Weight Impact Test

The falling weight impact test provided information about the behavior of the polyamide composites under dynamic loading. In the test, a tup of a given diameter was dropped from a preset height onto a flat test piece placed on a circular support surface, gripped with a clamping ring. The weight of the tup varied depending on the equipment and the required load. The conceptual arrangement of the falling weight impact test is described in ISO 6603.

Total energy $(E_{\rm total})$, maximum energy $(E_{\rm Fmax})$, and the 50% reduction $(1/2\,F_{\rm max})$ of the maximum force $(F_{\rm max})$ were determined from the curve recorded by the data acquisition unit. Perforation energy is obtained as the ratio of $E_{\rm total}$ to the thickness of the tested sheetlike product, corresponding to a 50% reduction in the maximum force $(1/2\,s_{\rm max})$. The ductility index (DI), a dimensionless indicator of the toughness of failure, was determined with Equation (4).

$$DI = \frac{E_{\text{total}} - E_{F \text{ max}}}{E_{\text{total}}} [-]$$
 (4)

With the thickness of the test specimens, the perforation energy can be determined with Equation (5):

$$E_{\text{perf.}} = \frac{E_{\text{total}}}{v} \tag{5}$$

where $E_{\rm perf}$ is the perforation energy (J/mm), ν is specimen thickness (mm), $E_{\rm total}$ is the energy up to the first zero transition (J).

We used an Instron/Ceast Fractovis 9350 impactor for the impact test with a dart with a hemispherical tip and a diameter of 20 mm. Drop height was 1 m.

2.3.6 | Charpy Tests

Charpy impact tests were carried out according to ISO 179-1:2023 with a Ceast Resil Impactor Junior impactor with a 15 J hammer. The tests showed the effect of fiber reinforcement on dynamic properties. The dimensions of the unnotched specimens were $10\times80\,\mathrm{mm}$ (thickness differs from the standard due to manufacturing technology), and support length was 62 mm. In this test, we only measured specific impact work. It was calculated with Equation (6):

$$KCV = \frac{K - K_0}{A_0} \tag{6}$$

where KCV is specific impact work [J/cm²], K is fracture energy [J], K_0 is idle energy [J], A_0 is the cross-section [cm²].

2.3.7 | HDT Tests

In the heat deflection temperature (HDT) test, the specimen was immersed in silicone oil and subjected to three-point bending

while the temperature of the silicone oil was raised. The test was carried out according to ISO 75-3 with a Ceast HV3 6911.000 machine and a load of 2.5 MPa, which applies to continuous fiber–reinforced plastic and high-strength thermoset composites. The same specimen geometry was used for the test as in the Charpy tests, with a support spacing of 64mm. The maximum allowable deflection was 0.54mm. The initial temperature of the silicone oil was 30°C, the heating rate was 120°C/h, and the maximum temperature was 300°C. The loaded specimen creeps most during the first 5 min. Therefore, a waiting time of 300s is required before the heating phase.

2.3.8 | Scanning Electron Microscopy (SEM)

A fracture surface of the specimens was examined by SEM. The specimens were fixed with electrically conductive adhesive and were gold-plated before the analysis for better test results. Images were recorded at a magnification of $50\times$, $500\times$, $1000\times$, and $2000\times$ with a JEOL JSM-6380LA (Jeol Ltd.) microscope.

3 | Results and Discussion

3.1 | Fiber Content

Table 2 summarizes fiber content measurement. Fiber contents can be considered realistic since the 4-layer sample is double the size of the 2-layer sample, and the 6-layer sample is not much larger. This minor difference was because mold size (cavity thickness) was the same, so in the CF2 sample, the matrix material filled the remaining space, but infiltration was not adequate when 6 layers were used.

3.2 | Permeability

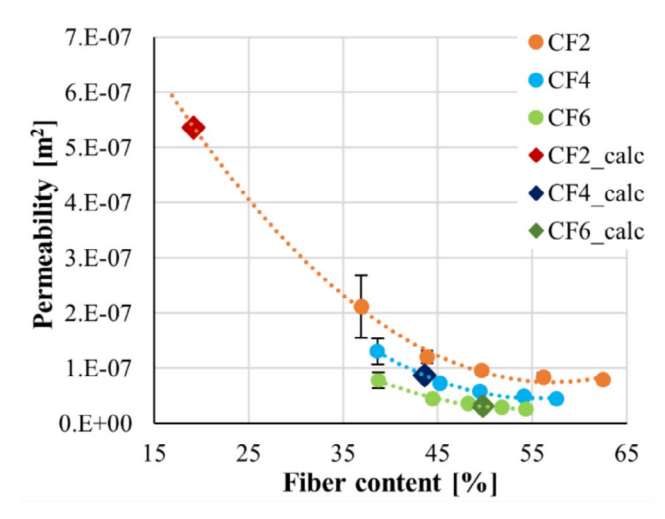
Permeability was measured for 2, 4, and 6 layers of carbon fiber fabric. Different flow rates were used for every sample, from 2 L/min to 50 L/min. From these, permeability was calculated with the procedure described previously. We repeated this process with a compression force of 300, 1000, 1800, 2800, and 3700 N in order to change the apparent fiber content. After that, average permeability was calculated for every number of layers at different force values (Figure 5). In Figure 5, we plotted the calculated permeability of the different structures based on the equations of the trend lines and the actual fiber contents of the different

TABLE 2 | Fiber content measurement results.

		Ash content	Fiber content
Name	Sample type	[m%]	[m%]
PA_mx	Pure matrix	0.6	0.0
CF2	2-layer sample	19.8	19.2
CF4	4-layer sample	44.2	43.6
CF6	6-layer sample	50.4	49.8

structures (CF2_calc, CF4_calc, and CF6_calc) calculated in the previous chapter.

The figure shows that permeability decreases as fiber content and the number of layers increase. Permeability ranged between 10^{-7} and 10^{-8} m², which is consistent with literature data measured in similar configurations [33]. Due to the high clamping force, uneven filling can occur in the case of 6 layers due to the low porosity, as shown in Figure 2c. From the



 $\mbox{\bf FIGURE 5} \quad | \quad \mbox{Permeability of pure carbon fabric as a function of fiber content.}$

results, we can assume that the 2- and 4-layer samples will have good impregnation, but the 6-layer sample could have some problems because of the low permeability at higher compression forces.

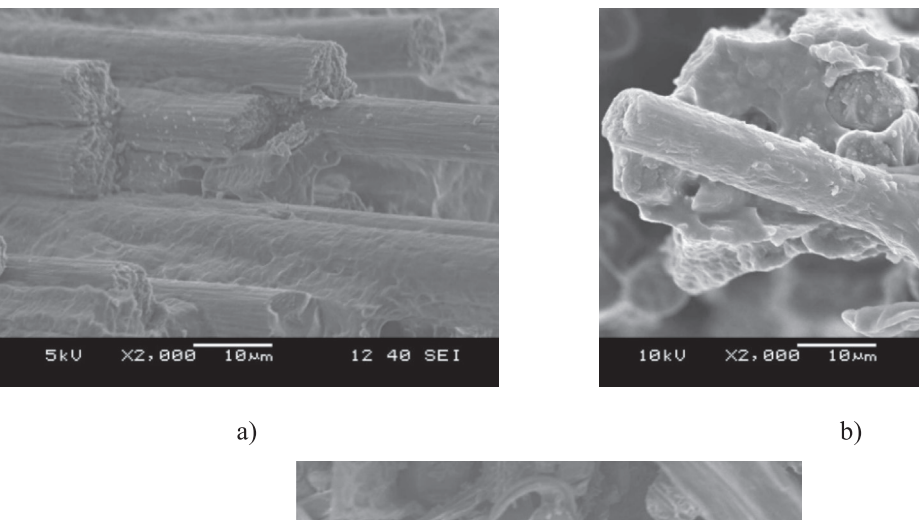
3.3 | SEM

We examined fabric saturation, and the nature of the behavior of the samples during fracture. Figure 6a shows the fracture surface of specimen CF2. The images show that the impregnation of the fabrics is good, as the carbon fibers within the rovings are surrounded by the matrix material, even in the innermost parts of the sample. The adhesion of the reinforcement structure is adequate, as in an ideal case, the mode of destruction of the composites is the rupture of the fibers, which are found in many places in the sample. This was an expected result based on the tensile test, which was carried out on the samples before the SEM examination.

Figure 6b shows that in the case of the 4-layer samples, the fabric was also impregnated well, with the matrix material surrounding the PA6 entirely. The typical failure in this case was also fiber breakage. We only observed fiber pullout in some instances. This explains the tensile test results, where we measured excellent tensile strength and modulus for the 4-layer samples.

In the case of the 6-layer samples (Figure 6c), adhesion is not good. Most of the fibers are almost completely dry, and

09 40 SEI



5kV X2,888 10 mm 11 48 SEI

FIGURE 6 | SEM images of the 2- (a), 4- (b), and 6-layer (c) samples at a magnification of 2000×.

infiltration was inadequate. This resulted in poorer mechanical properties, as the tensile tests proved.

The 2- and 4-layer samples had the best fiber–matrix bonding, filling, and impregnation, as evidenced by their good mechanical properties.

3.4 | Tensile Tests

Figure 7a shows the typical failures of the specimens during the tensile tests. Two types of specimens with different fiber orientations were tested. In the first case, the fibers are perpendicular and parallel to the load direction and are labeled CF2_90, CF4_90 and CF6_90. For the second type, the fibers are locked at ±45° to the load direction and are labeled CF2_45, CF4_45 and CF6_45. We performed five tests for each sample type to determine tensile strength, modulus of elasticity and elongation at break. The impregnation of the 6-layer samples was not good enough to produce homogenous CF6_90 samples. Because of this, we left those samples out of this test series. Figure 7b shows the characteristic curves obtained from the tensile tests.

The most characteristic curves from the five tests were selected for comparison with each composite structure and the pure matrix. Compared to the matrix, the carbon fiber-reinforced composite specimens are more brittle, as elongation at break

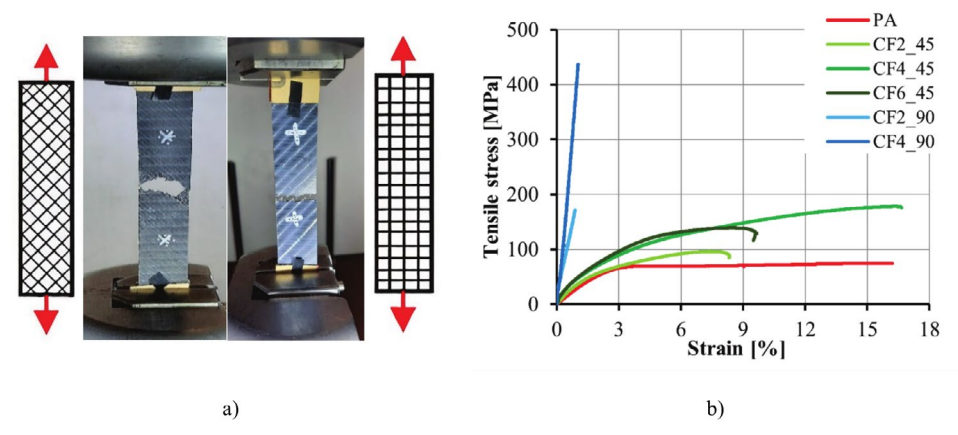


FIGURE 7 | ±45° (left) and 0/90° (right) test specimen (a); characteristic curves of tensile tests (b).

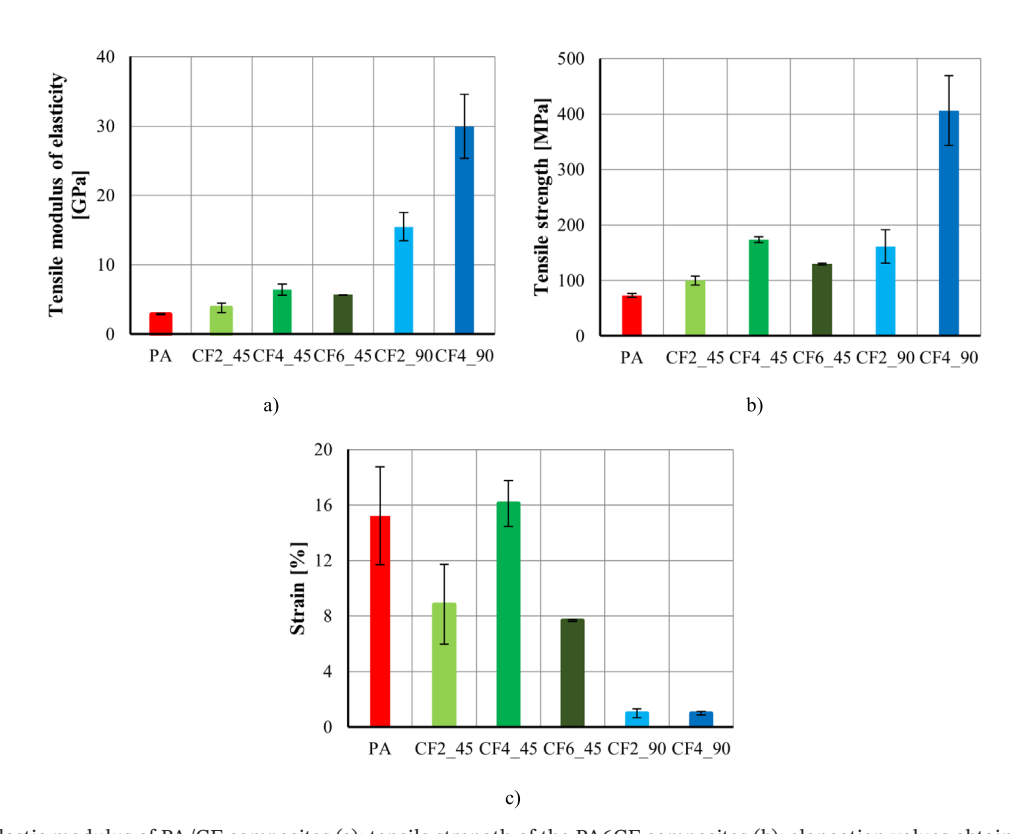
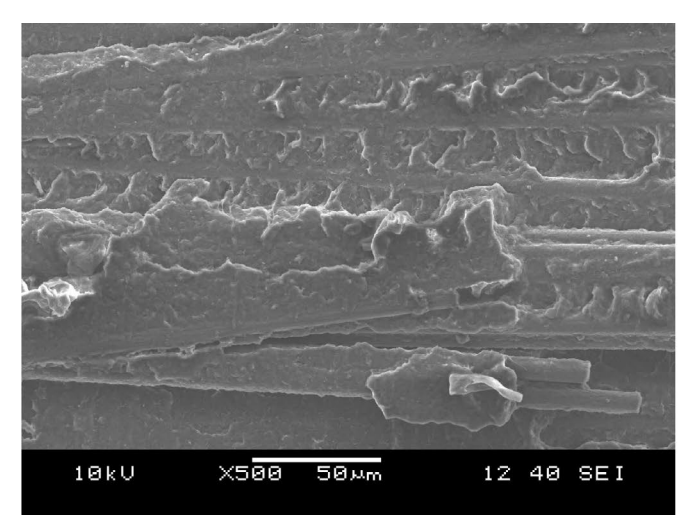


FIGURE 8 | Elastic modulus of PA/CF composites (a); tensile strength of the PA6CF composites (b); elongation values obtained from the tensile tests (c).



10kU X100 100µm 12 40 SEI

FIGURE 9 | SEM images of interlaminar shear test samples.

decreases and modulus and strength increase. The slopes of the curves for the tensile tests illustrate this. The only exception is CF4_45, which has elongation at break close to that of the pure matrix material. The 4-layer specimens show an exceptionally high elongation at break and strength due to the excellent interfacial adhesion and impregnation compared to the other specimens. The ±45° 2-layer samples had a tensile strength similar to that of the matrix material, and the tensile strength of the 2-layer 0/90° sample test was well below that of the 4-layer 0/90° sample. The highest tensile strength of the CF4_90 specimen was ~480 MPa. Tensile modulus ranges from 4 to 34 GPa as a function of fiber orientation and layer number. Compared to the 2-layer specimens, the 4-layer specimens had an almost 100% higher elastic modulus and elongation at break.

Large scatter in the case of composites is typical, as reproducibility depends on many factors. Furthermore, tests were carried out on samples taken from the beginning and the end of the flow path. This alone produces differences in mechanical properties. As we cut the 0/90° specimens from the sheets at an angle of 45°, specimen quality was poorer at the corners of the plates, which explains why some samples broke in or near the grip. Figure 8a–c shows the most important mechanical properties.

3.5 | Interlaminar Shear Test

For this test, six test specimens were prepared. The test can only be performed on composite samples with an even number of layers. Figure 4 shows a test specimen. The PA reference sample has no specific shear strength, but its tensile strength was 73 MPa. The average interlayer shear test results gave an interlayer shear strength of 39.19 MPa for the 4-layer samples. We examined only the CF4 samples because the CF2 samples have an extra matrix layer on the top of the samples, so they are not symmetric. The force maximum measured in the tensile tests was around 3500 N for the matrix material, while forces between 2100 and 3200 N were measured in the interlayer shear test. This confirms the SEM results in Figure 9—that the matrix was indeed sheared.

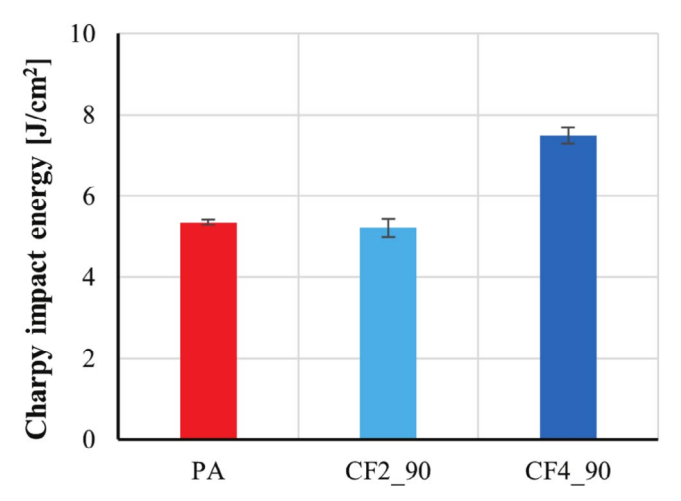


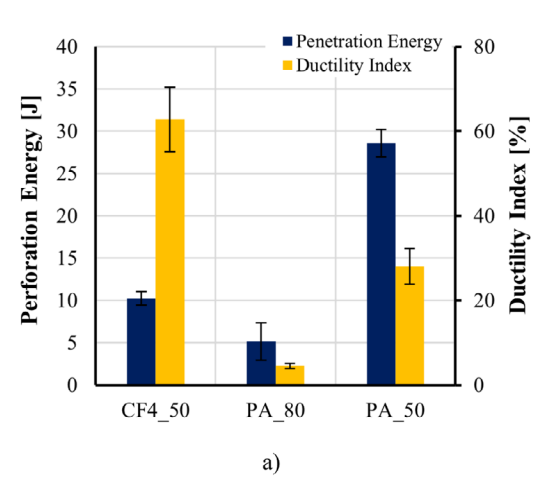
FIGURE 10 | Charpy impact test results.

3.6 | Dynamic Impact Tests

The hammer characteristics were set on the instrument; the idle energy of the hammer was measured, and only then were the test pieces inserted. Idle energy must always be subtracted from the estimated energy. Impact energy can be read directly from the machine during the test. The results are summarized in Figure 10.

In the case of composites, the standard requires that the test specimens be struck flatwise. The CF2_90 and CF4_45 specimens did not break when they were hit this way, so we could not test these samples. This shows that 45° fabrics are much tougher than 90° specimens. For the PA reference, specific impact energy was 5.3 J/cm². The impact energy of the CF2_90 samples (5.2 J/cm²) was almost the same. The 4-layer sample had a significantly higher impact energy of 7.5 J/cm².

The dynamic mechanical properties and the perforation energy of the composite specimens were also measured. The tests were carried out at room temperature. The impactor had a kinetic energy of 50J when the reinforced samples were tested and 80J



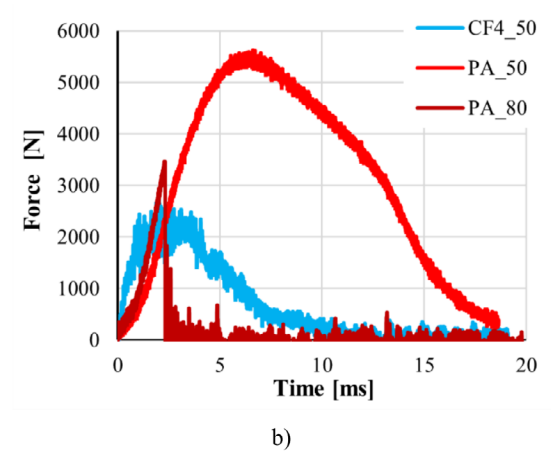


FIGURE 11 | Perforation energies and ductility indexes (a); force-displacement curves for falling weight impact testing (b).

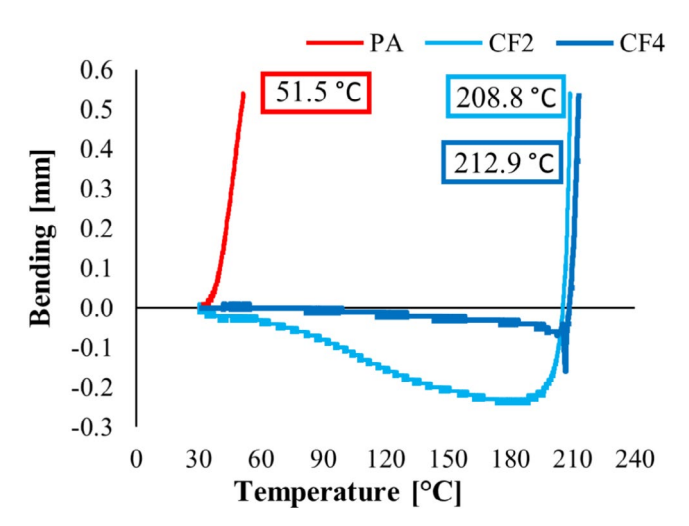


FIGURE 12 \mid HDT curves and temperatures of the 2- and 4-layer samples.

when the matrix material was tested. Higher energy was chosen for the PA6 matrix because the tip did not penetrate the specimen at 50 J. From the composite sheets, ten pieces of 80×80 mm specimens were prepared.

Figure 11a shows the perforation energies, which are the energy values per unit thickness of the samples. For clarity, we plotted the DIs as a percentage.

The fiber-reinforced samples exhibited ductile behavior. At these energies, they fractured in a brittle way; but for comparability, we wanted to include benchmarks. Figure 11b shows a typical curve from the falling weight tests. We examined the characteristic load forces as a function of tip displacement up to the first zero transition. The falling weight tests were performed at the center of the surface of the specimen. We cut out the samples from different parts of the manufactured sheets, which may have significantly influenced the results.

3.7 | HDT

The 6-layer samples could not be tested for HDT due to the impregnation problems. The two- and four-layer samples were cut

from the sheet with a fiber orientation of 0/90°. Their HDT was more than ~300% higher compared to that of the reference sample. The HDT of the four-layer samples was 4°C higher than that of the 2-layer samples. Figure 12 shows the HDT curves and the HDTs. The negative values of the curve could be due to the warped carbon fibers caused by thermal expansion. In addition, the 2-layer sample has a thicker matrix layer on one side, so there is a thermal expansion difference between the two sides, amplifying this effect.

4 | Conclusion

We produced continuous carbon fiber-reinforced composite structures with various stacking sequences and fiber orientations by T-RTM to comprehensively investigate the mechanical, thermal, and morphological properties of the structures. Before manufacturing, we conducted permeability tests for 2-, 4-, and 6-layer specimens to assess their feasibility for T-RTM processing. Based on the results, the 2-layer and 4-layer samples were deemed manufacturable, while potential processing issues were identified with the 6-layer specimens.

During manufacturing, fabric layers were placed into the mold before each cycle, followed by the injection of caprolactam, activator, and catalyst. Polymerization subsequently occurred, resulting in carbon fiber–reinforced PA6 composite sheets. The 2-layer and 4-layer specimens exhibited excellent quality and impregnation, whereas in the 6-layer samples—especially in the middle—there were dry fiber regions. The 2-layer samples showed a higher degree of warpage compared to the 4-layer samples due to their asymmetry. This asymmetry was due to the fact that the mold cavity with a nominal thickness of 2 mm was not completely filled by the 2 layers of fabric. Thus, the cross-section of the sample was richer in matrix material on one side. After manufacturing, test specimens were cut in two different orientations for subsequent evaluation.

The first step involved fiber content analysis to verify the accuracy of the permeability measurements and their consistency with actual processing conditions. The measured fiber contents were $19.2\,\text{m/m}\%$ for CF2, $43.6\,\text{m/m}\%$ for CF4, and $49.8\,\text{m/m}\%$ for CF6 samples.

Tensile and interlaminar shear tests were also performed. The tensile tests revealed a significant increase in tensile strength for CF4_90 specimens, reaching 480 MPa—nearly a sevenfold increase compared to the reference PA specimens (70 MPa). SEM analysis of fractured specimens confirmed the assumed excellent impregnation for CF2 and CF4 samples, while poor impregnation was evident in CF6 specimens. Interlaminar shear testing further proved the high quality of CF4 laminates, with a remarkably high interlaminar shear strength of 39.19 MPa.

HDT tests showed that the HDT of fiber-reinforced specimens was more than 150°C higher than that of the reference PA specimens.

Dynamic impact tests, including Charpy and falling weight impact tests, indicated that the manufactured specimens had high impact resistance and were suitable for load-bearing applications.

In conclusion, the mechanical and dynamic mechanical tests showed that the composite structures reinforced with continuous carbon fibers we produced with short cycle times were high quality. The T-RTM technology enables continuous cyclic production, making it a viable solution for industrial applications.

Author Contributions

Péter Széplaki: investigation, visualization, data curation, writing – original draft. **Szabolcs Hajagos:** investigation, data curation. **Szabolcs Krizsma:** investigation. **Béla Zink:** conceptualization, methodology, supervision. **András Suplicz:** conceptualization, investigation, methodology, data curation, supervision, writing – review and editing, project administration, visualization.

Acknowledgments

We wish to thank TOOL-TEMP HUNGÁRIA KFT for the temperature controllers.

Conflicts of Interest

The authors declare no conflicts of interest.

Data Availability Statement

The data that support the findings of this study are available from the corresponding author upon reasonable request.

References

- $1. \ "Plastics the Facts 2024." \ https://plasticseurope.org/knowledge-hub/plastics-the-fast-facts-2024/.$
- 2. O. V. Semperger and A. Suplicz, "The Effect of the Parameters of T-RTM on the Properties of Polyamide 6 Prepared by in Situ Polymerization," *Materials* 13, no. 4 (2020): 1–11, https://doi.org/10.3390/ma130 10004.
- 3. W. Du, I. N. Orbulov, P. Tamás-Bényei, and C. Kádár, "Mechanical Behavior of Layered Composite Structures of Aluminum Foam Partially Filled With Polyamide," *Periodica Polytechnica, Mechanical Engineering* 69 (2025): 164–170, https://doi.org/10.3311/PPme.40446.
- 4. O. Nuyken and S. D. Pask, "Ring-Opening Polymerization—An Introductory Review," *Polymers* 5, no. 2 (2013): 361–403, https://doi.org/10.3390/polym5020361.

- 5. J. Lee, J. W. Lim, and M. Kim, "Effect of Thermoplastic Resin Transfer Molding Process and Flame Surface Treatment on Mechanical Properties of Carbon Fiber Reinforced Polyamide 6 Composite," *Polymer Composites* 41 (2020): 1190–1202, https://doi.org/10.1002/pc. 25445.
- 6. L. Lewerdomski and C. Schütz, "Interfacial Adhesion Optimization Using 2-C Silane Compounds During the T-RTM Process," *Lightweight Design Worldwide* 12 (2019): 38–43, https://doi.org/10.1007/s41777-019-0050-3.
- 7. M. Thomassey, B. P. Revol, F. Ruch, J. Schell, and M. Bouquey, "Interest of a Rheokinetic Study for the Development of Thermoplastic Composites by T-RTM," *Universal Journal of Materials Science* 5 (2017): 15–27, https://doi.org/10.13189/ujms.2017.050103.
- 8. T. Ageyeva, I. Sibikin, and J. Karger-Kocsis, "Polymers and Related Composites via Anionic Ring-Opening Polymerization of Lactams: Recent Developments and Future Trends," *Polymers* 10, no. 4 (2018): 357, https://doi.org/10.3390/polym10040357.
- 9. R. Wendel, B. Thoma, and F. Henning, "Influence of Water During Manufacturing of aPA6 in the Thermoplastic RTM Process," in *Proceedings of the Conference 2017 of the Polymer Processing Society*, Cancun, Mexico, (10–14 December 2017), 3.
- 10. J. Herzog, R. Wendel, P. G. Weidler, M. Wilhelm, P. Rosenberg, and F. Henning, "Moisture Adsorption and Desorption Behavior of Raw Materials for the T-RTM Process," *Journal of Composites Science* 5, no. 1 (2021): 12, https://doi.org/10.3390/jcs5010012.
- 11. W. H. Lin, C. M. Wu, S. Chaudhuri, T. C. An, and P. H. Huang, "Hygroscopic Elongation of Moisture-Responsive Polyamide 6 Fibers Copolymerized With Polyetherdiamine and Adipic Acid," *Express Polymer Letters* 18, no. 5 (2024): 475–486, https://doi.org/10.3144/expresspolymlett.2024.35.
- 12. K. S. Boparai, R. Singh, F. Fabbrocino, and F. Fraternal, "Thermal Characterization of Recycled Polymer for Additive Manufacturing Applications," *Composites Part B, Engineering* 106 (2016): 42–47, https://doi.org/10.1016/j.compositesb.2016.09.009.
- 13. C.-C. Höhne, R. Wendel, B. Käbisch, T. Anders, F. Henning, and E. Kroke, "Hexaphenoxycyclotriphosphazene as FR for CFR Anionic PA6 via T-RTM: A Study of Mechanical and Thermal Properties," *Fire and Materials* 41 (2017): 291–306, https://doi.org/10.1002/fam.2375.
- 14. N. Zaldua, J. Maiz, A. de la Calle, et al., "Nucleation and Crystallization of PA6 Composites Prepared by T-RTM: Effects of Carbon and Glass Fiber Loading," *Polymers* 11, no. 10 (2019): 1680, https://doi.org/10.3390/polym11101680.
- 15. A. Toldy, "Safe and Sustainable-by-Design: Redefining Polymer Engineering for a Greener Future," *Express Polymer Letters* 19, no. 4 (2025): 350, https://doi.org/10.3144/expresspolymlett.2025.25.
- 16. C. W. Choi, J. W. Jin, H. Lee, M. Huh, and K. W. Kang, "Optimal Polymerization Conditions in Thermoplastic-Resin Transfer Molding Process for Mechanical Properties of Carbon Fiber-Reinforced PA6 Composites Using the Response Surface Method," *Fibers and Polymers* 20 (2019): 1021–1028, https://doi.org/10.1007/s12221-019-8901-4.
- 17. B. J. Kim, S. H. Cha, and Y. B. Park, "Ultra-High-Speed Processing of Nanomaterial-Reinforced Woven Carbon Fiber/Polyamide 6 Composites Using Reactive Thermoplastic Resin Transfer Molding," *Composites Part B: Engineering* 143 (2018): 36–46, https://doi.org/10.1016/j.compositesb.2018.02.002.
- 18. M. X. Li, H. L. Mo, Y. Ren, and S. W. Choi, "Carbon Fiber-Reinforced Polyamide 6 Composites Formed by In Situ Polymerization—Experimental and Numerical Analysis of the Influence of Polymerization Temperature," *Coatings* 12, no. 7 (2022): 947, https://doi.org/10.3390/coatings12070947.
- 19. M. Wilhelm, R. Wendel, M. Aust, P. Rosenberg, and F. Henning, "Compensation of Water Influence on Anionic Polymerization of

- ε-Caprolactam: 1. Chemistry and Experiments," *Journal of Composites Science* 4, no. 1 (2020): 7, https://doi.org/10.3390/jcs4010007.
- 20. J. H. Lee, S. M. Son, J. J. Yoo, S. W. Kim, J. W. Yi, and D. G. Seong, "Thermoplastic Resin Transfer Molding of Carbon Fiber Reinforced Polyamide 6 Composite With the Improved Processability Using Zeolite Particle," *Korea-Australia Rheology Journal* 35, no. 1 (2023): 39–45, https://doi.org/10.1007/s13367-023-00051-4.
- 21. N. Dencheva, A. S. Sampaio, F. M. Oliveira, A. S. Pouzada, A. M. Brito, and Z. Denchev, "Preparation and Properties of Polyamide-6-Based Thermoplastic Laminate Composites by a Novel In-Mold Polymerization Technique," *Journal of Applied Polymer Science* 131, no. 8 (2014): app.40083, https://doi.org/10.1002/app.40083.
- 22. N. Dencheva, Z. Denchev, A. S. Pouzada, A. S. Sampaio, and A. M. Rocha, "Structure–Properties Relationship in Single Polymer Composites Based on Polyamide 6 Prepared by In-Mold Anionic Polymerization," *Journal of Materials Science* 48 (2013): 7260–7273, https://doi.org/10.1007/s10853-013-7546-8.
- 23. J. J. Murray, T. Allen, S. Bickerton, et al., "Thermoplastic RTM: Impact Properties of Anionically Polymerised Polyamide 6 Composites for Structural Automotive Parts," *Energies* 14, no. 18 (2021): 5790, https://doi.org/10.3390/en14185790.
- 24. J. J. Murray, C. Robert, K. Gleich, E. D. McCarthy, and C. M. Ó. Brádaigh, "Manufacturing of Unidirectional Stitched Glass Fabric Reinforced Polyamide 6 by Thermoplastic Resin Transfer Moulding," *Materials & Design* 189 (2020): 108512, https://doi.org/10.1016/j.matdes. 2020.108512.
- 25. C. Gomez, D. Salvatori, B. Caglar, R. Trigueira, G. Orange, and V. Michaud, "Resin Transfer Molding of High-Fluidity Polyamide-6 With Modified Glass-Fabric Preforms," *Composites Part A: Applied Science and Manufacturing* 147 (2021): 106448, https://doi.org/10.1016/j.compositesa.2021.106448.
- 26. K. van Rijswijk, H. E. N. Bersee, W. F. Jager, and S. J. Picken, "Optimisation of Anionic Polyamide-6 for Vacuum Infusion of Thermoplastic Composites: Choice of Activator and Initiator," *Composites Part A, Applied Science and Manufacturing* 37, no. 6 (2006): 949–956, https://doi.org/10.1016/j.compositesa.2005.01.023.
- 27. Zs. Osváth, A. Szőke, Sz. Pásztor, L. Závoczki, G. Szarka, and B. Iván, "Recent Advances in the Synthesis and Analysis of Polyamide 6 and Products Therefrom: From Polymerization Chemistry of ε-Caprolactam to Thermoplastic Resin Transfer Molding (T-RTM)," *Academic Journal of Polymer Science* 4, no. 1 (2020): 118–122, https://doi.org/10.19080/AJOP.2020.04.555629.
- 28. O. V. Semperger, P. Pomlényi, and A. Suplicz, "In-Mold Coating Technology for T-RTM Process," *Polimerek* 7, no. 6 (2021): 186–192.
- 29. M. Valente, I. Rossitti, and M. Sambucci, "Thermoplastic Composite Materials Approach for More Circular Components: From Monomer to in Situ Polymerization, a Review," *Journal of Composites Science* 6, no. 5 (2022): 132, https://doi.org/10.3390/jcs6050132.
- 30. T. Ageyeva, I. Sibikin, and J. G. Kovács, "A Review of Thermoplastic Resin Transfer Molding: Process Modeling and Simulation," *Polymers* 11, no. 10 (2019): 1555, https://doi.org/10.3390/polym11101555.
- 31. Zs. Kovács, Á. Pomázi, and A. Toldy, "The Flame Retardancy of Polyamide 6—Prepared by in Situ Polymerisation of ε-Caprolactam—For T-RTM Applications," *Polymer Degradation and Stability* 195 (2022): 109797, https://doi.org/10.1016/j.polymdegradstab.2021.109797.
- 32. R. Pomeroy, S. Grove, J. Summerscales, Y. Wang, and A. Harper, "Measurement of Permeability of Continuous Filament Mat Glass-Fibre Reinforcements by Saturated Radial Airflow," *Composites Part A: Applied Science and Manufacturing* 38, no. 5 (2007): 1439–1443, https://doi.org/10.1016/j.compositesa.2006.11.011.
- 33. G. W. C. Kaye and T. H. Laby, *Tables of Physical and Chemical Constants and Some Mathematical Functions* (Longmans, Green and Company, 1928).